Supplementary Information

Au nanoparticles decorated β-Bi$_2$O$_3$ as highly-sensitive SERS substrate for detection of methylene blue and methyl orange

Binbin Chen[a,1], Lizhu Fan[b,1], Viktoria Golovanova[c],Chunyu Li[f], Kaiwen Wang[a], Jinshu Wang[e], Dawei Pang[a]*, Zhouhao Zhu[d]**, Peijie Ma[a]***

[a] Beijing Key Lab of Microstructure and Property of Advanced Materials, College of Materials Science & Engineering, Beijing University of Technology, Beijing, 100124, China

[b] National Key Laboratory of Integrated Circuits and Microsystems, Chongqing, 401332, China

[c] South-Ukrainian National University, Staroportofrankovskaya Str. 26, 65008, Odessa, Ukraine

[d] College of Physics and Center of Quantum Materials and Devices, Chongqing University, Chongqing, 401331, China

[e] School of Public Health and Health Sciences, Tianjin University of Traditional Chinese Medicine, Tianjin 301617, China

[f] Institute of Physical Chemistry, Friedrich Schiller University Jena, Helmholtzweg 4, 07743, Jena, Germany

* Corresponding author.

** Corresponding author.

*** Corresponding author.

E-mail addresses: gavinpang@bjut.edu.cn (D. Pang), zhuzhouhao98@foxmail.com (Z. Zhu), peijiema@bjut.edu.cn (P. Ma).

[1] These authors contributed equally to this work.

Calculation of enhancement factors (EF)

Enhancement Factor (EF), as an important parameter, is evaluated to quantify the enhancement effect of a substrate using the following formula [1]:

$$\text{EF} = \frac{I_S N_{bulk}}{I_R N_{surf}}. \qquad \text{Eq. (1)}$$

In the equation, I_S and I_R represent the Raman signal intensities of the molecule MB with and without the presence of the SERS-enhancing substrate, respectively. N_{bulk} is the average number of MB molecules detected in the absence of SERS measurements, and N_{surf} is the average number of MB molecules detected in SERS measurements. The calculation method for N_{bulk} is as follows:

$$N_{bulk} = \frac{A_{laser} \times h \times \rho}{M} \times N_A. \qquad \text{Eq. (2)}$$

In the equation, A_{laser}, h, ρ, and M represent the laser spot area, focal length, density of the solid analyte, and relative molecular mass, respectively. N_A refers to Avogadro's number. The calculation for $N_{surface}$ is as follows:

$$N_{surface} = \frac{C \times V}{A_{substrate}} \times N_A \times A_{laser}. \qquad \text{Eq. (3)}$$

In the equation, C, V, and $A_{substrate}$ represent the concentration, volume of the analyte solution, and substrate area, respectively. N_A refers to Avogadro's number, and A_{laser} represents the area of the laser spot.

Therefore, EF can be calculated as follows:

$$EF = \frac{I_S}{I_R} \times \frac{N_{bulk}}{N_{surf}} = \frac{I_S}{I_R} \times \frac{h \times \rho \times A_{substrate}}{M \times C \times V}. \qquad \text{Eq. (4)}$$

EF calculations for MB:

For β-Bi$_2$O$_3$ substrate, I_R =1523 (a.u.), h = 0.2 (mm), ρ = 0.6 (g/cm^3), M = 356 (g/mol), $A_{substrate}$ = 4 (mm^2), V = 10 (μL), C =10^{-7} M, and I_S = 1986 (a.u.) (at 1624 cm^{-1}), the EF is estimated to be 3.94 × 10^6.

For 5.20%Au/Bi$_2$O$_3$ sample, I_R = 1523 (a.u.), h = 0.2 (mm), ρ = 0.6 (g/cm^3), M = 356 (g/mol), $A_{substrate}$ = 4 (mm^2), V = 10 (μL), C =10^{-7} M, and I_S = 4649 (a.u.) (at 1624 cm^{-1}), the EF is estimated to be 9.22 × 10^6.

The calculation for MO is similar to that for MB, and it is calculated：

For β-Bi$_2$O$_3$ sample, EF is estimated to be 2.96 × 10^4.

For 5.20%Au/Bi$_2$O$_3$ sample, EF is estimated to be 1.15 × 10^5.

Calculation of mass fractions from ICP-AES

A 150mg powder sample of 5.20%Au/Bi_2O_3 was taken and dissolved in 4mL aqua regia. The solution was then diluted with distilled water to a final volume of 15mL. Subsequently, it was further diluted 1000 times. The measurement results using ICP-AES showed that the concentration of Au was 0.520mg/L, which corresponds to a mass of 7.8mg of Au (m = C × V=7.8mg). The mass fraction of Au was calculated as ω = m/m_0 = 5.20%. Similarly, when 2.80%Au/Bi_2O_3 and 10.1%Au/Bi_2O_3 samples were processed using the same method and their Au contents were measured, the respective concentrations were found to be 0.280mg/L and 1.010mg/L. This resulted in mass fractions of Au of 2.80% and 10.1% for 2.80%Au/Bi_2O_3 and 10.1%Au/Bi_2O_3, respectively.
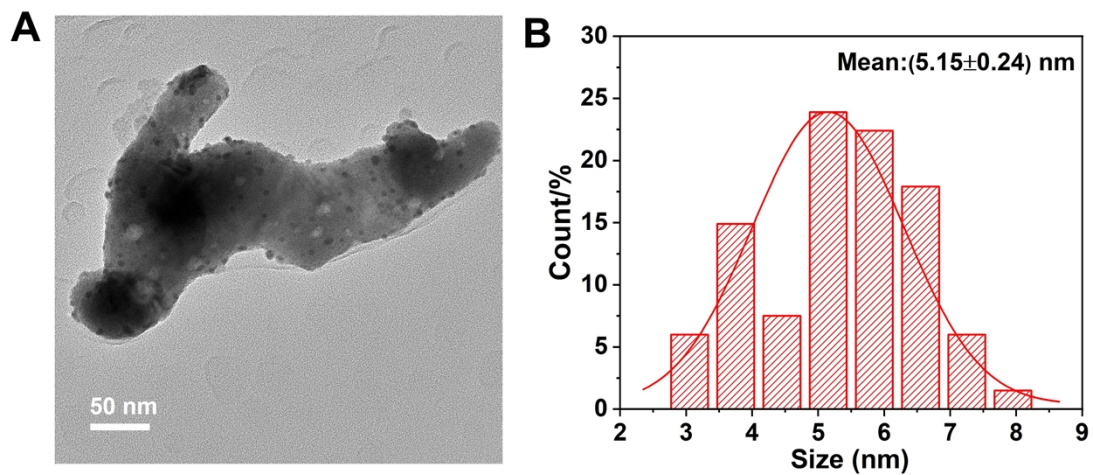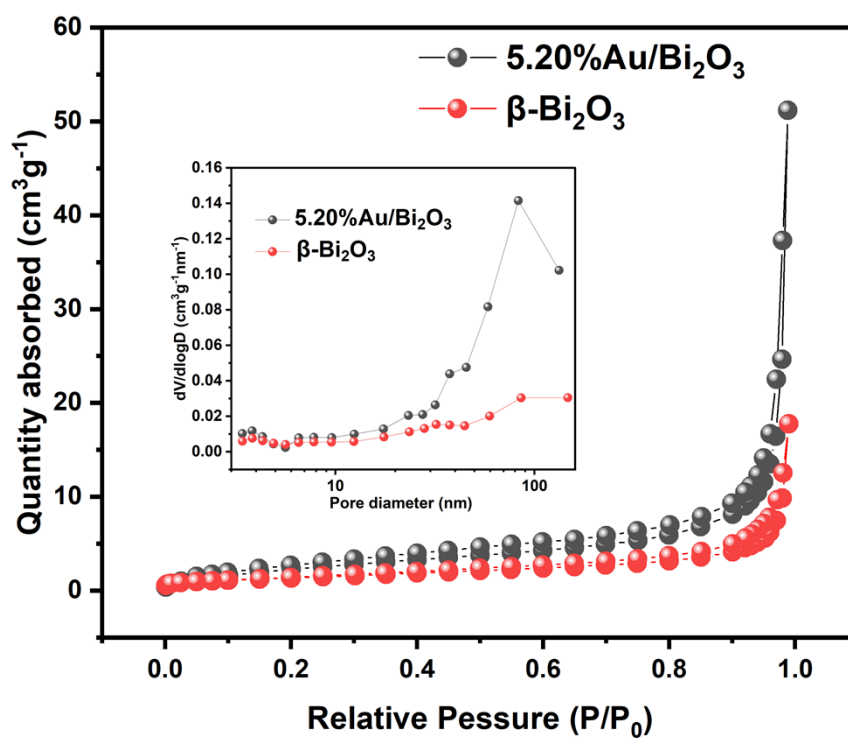
Fig. S1 Size distribution histograms of Au NPs on 5.20%Au/Bi_2O_3.
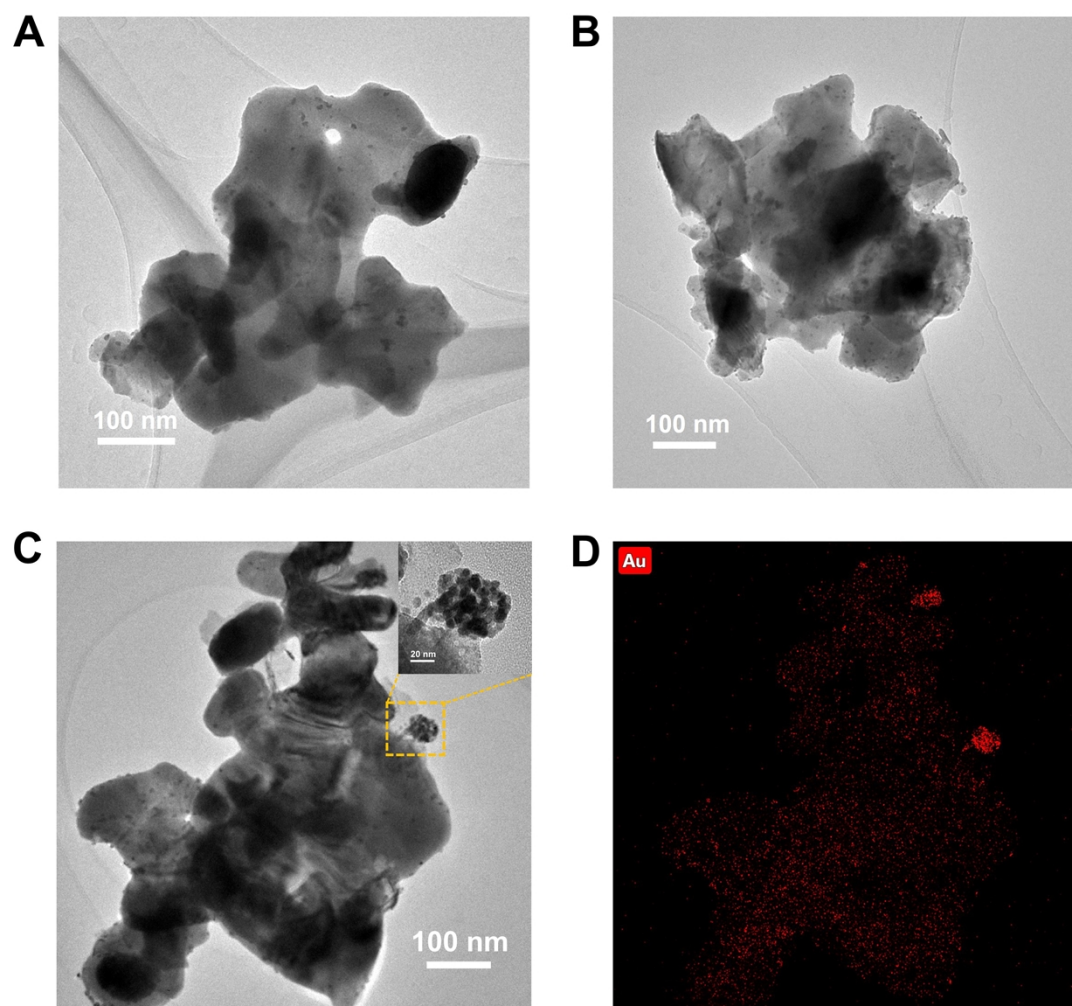
Fig. S2 TEM images of (A) 2.80%Au/Bi_2O_3, (B) 5.20%Au/Bi_2O_3 and (C) 10.1%Au/Bi_2O_3 (Insert is an enlarged view of the dotted box in (C)). (D) Elemental mapping image of Au of 10.1%Au/Bi_2O_3.
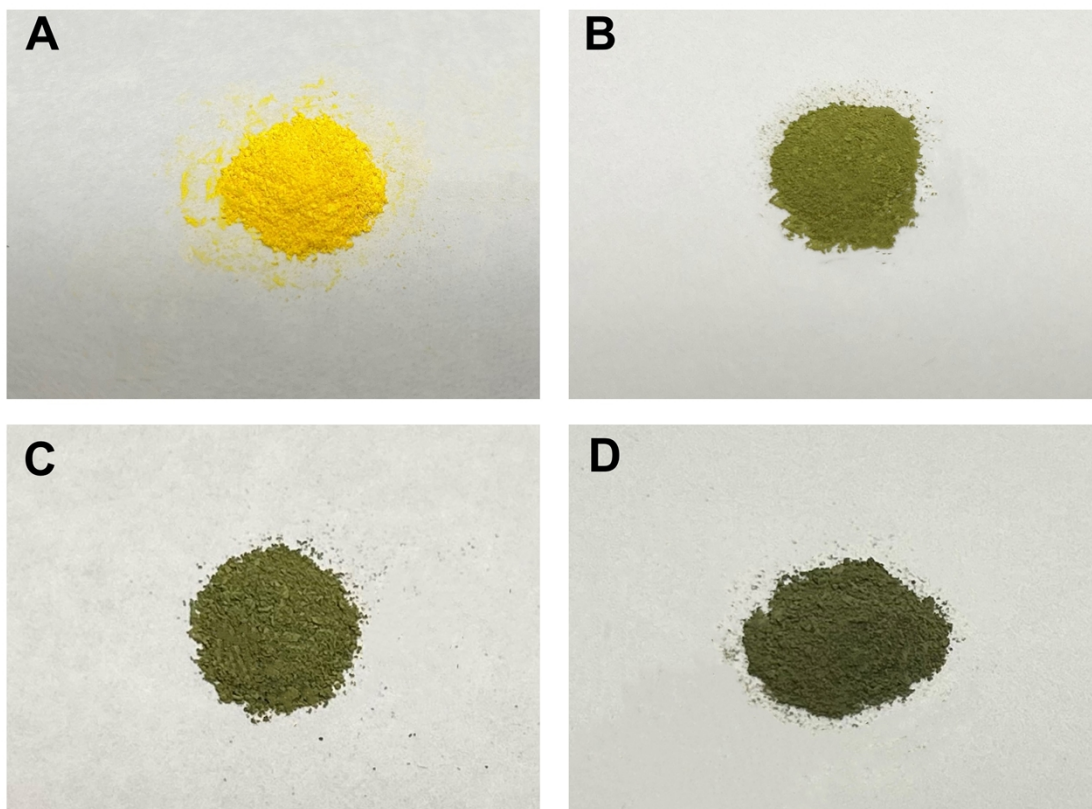
Fig. S3 Photos taken by iphone of (A) β-Bi$_2$O$_3$, (B) 2.80%Au/Bi$_2$O$_3$, (C) 5.20%Au/Bi$_2$O$_3$ and (D) 10.1%Au/Bi$_2$O$_3$.

Fig. S4 Nitrogen adsorption-desorption isotherms of β-Bi$_2$O$_3$ and 5.20%Au/Bi$_2$O$_3$ (The

inset is pore-size distributions).
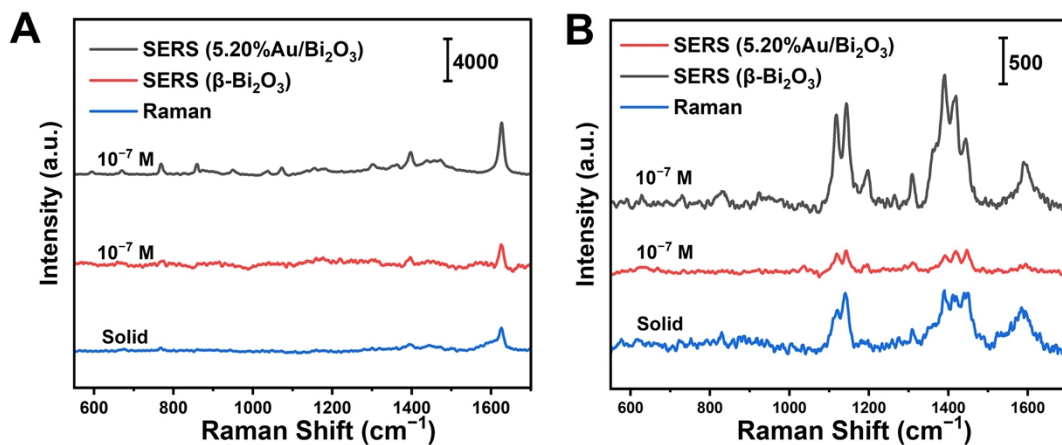
Fig. S5 Normal Raman spectra and SERS spectra of (A) MB and (B) MO.
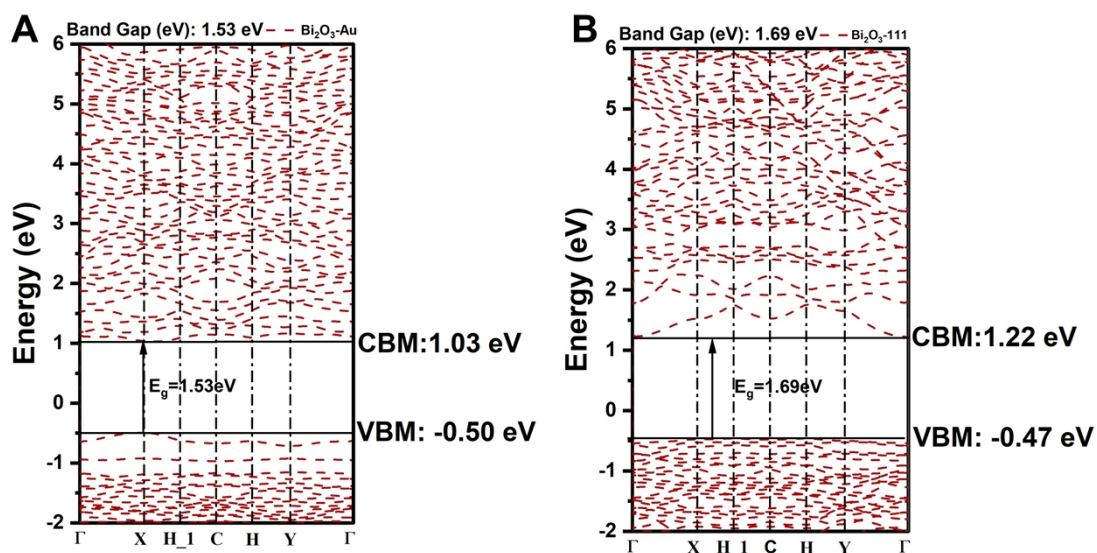
Fig. S6 Calculated band structures of (A) 5.20%Au/Bi_2O_3 and (B) β-Bi_2O_3.
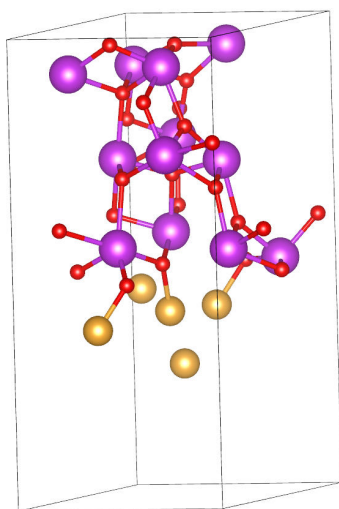
Fig. S7 Optimized model of 5.20%Au/Bi_2O_3 based on DFT calculation results.
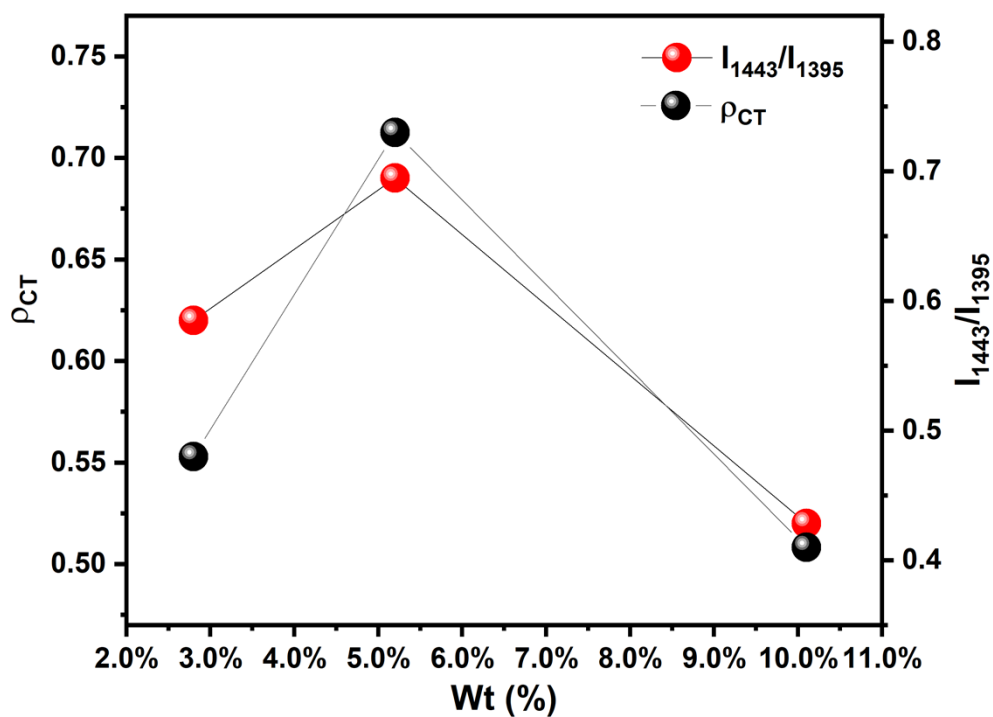
Fig. S8 Degree of charge transfer (ρ_{CT}) in the composites and the SERS intensity ratio between the modes at 1443 cm^{-1} (b_2) and 1395cm^{-1} (a_1) as a function of the load mass of Au NPs on β-Bi_2O_3.

Table S1. Mode assignment of the Raman peaks for MB.[2,3]

Normal Raman (cm $^{-1}$)	SERS (cm $^{-1}$)	Mode assignment
503	594	δ(C-S-C)
	669	β(C-H)
776	769	β(C-H)
862	858	β(C-H)
	899	β(C-H)
951	950	β(C-H)
1036	1038	β(C-H)
1073	1071	β(C-H)
	1153	β(C-H)
	1179	ν(C-N)
1305	1300	α(C-H)
1398	1395	ν_{sym}(C-N)
1437	1443	ν_{asym}(C-N)
1474	1468	ν_{asym}(C-N)
1625	1624	ν(C-C)

ν=stretching, α= ring deformation, β=bending and δ=skeletal deformation.

Table S2. Mode assignment of the Raman peaks for MO.[4]

Normal Raman (cm^{-1})	SERS (cm^{-1})	Peak assignment
828	831	β(C–H) + β(C–C) + ν(C–C)
921	925	ν(C–C)
1026	1025	β(C–C)
1122	1112	β(C–C)
1143	1144	β(C–C) + ν(C–C) + β(C–N)
1194	1196	ν(C–C) + β(C–C) + β(C–H)
1311	1313	ν(C–C) + β(C–H)
1362	1364	ν(C–C)
1396	1389	ν(N–N) +
1413	1410	ν(N–N)
1422	1422	ν(C–C)
1442	1444	ν(C–C) + β(C–H)
1590	1589	ν(C=C) + β(C=C)

ν=stretching and β=bending.

Table S3. Performance comparison of SERS semiconductor materials for the detection of MB.

Materials	Analyte molecules	LOD(M)	EF	
MoO_2/GO	MB	10^{-8}	/	1
S-MoO_2	MB	10^{-8}	/	2
TiO_2–PCC	MB	7.21×10^{-8}	3.63×10^4	3
$CdSe$-TiO_2 IOS	MB	7×10^{-9}	1.46×10^5	4
F_4TCNQ/MoS_2	MB	10^{-10}	2.531×10^6	5
MoO_3/MoO_2	MB	10^{-9}	1.4×10^5	6
SnS_2	MB	10^{-13}	3.0×10^8	7
$Mo_{1-x}W_xS_2$	MB	10^{-8}	/	8
β-Bi_2O_3	MB	10^{-9}	5.5×10^6	this work

1 molybdenum oxide and graphene oxide nanocomposite.[5]

2 sulfur-doped MoO_2 nanospheres.[6]

3 TiO_2-coated photonic crystal capillary.[7]

4 CdSe-sensitized TiO_2 composite film with inverse opal structure.[8]

5 F4TCNQ nanostructures grown on a 2D MoS_2 flake.[9]

6 MoO_3/MoO_2 nanosheets.[10]

7 SnS2 microspheres.[11]

8 $Mo_{1-x}W_xS_2$ nanosheets.

Table S4. Performance comparison of SERS noble metal loaded composites for the detection of MB.

Materials	Noble metal(wt%)	Analyte molecules	LOD(M)	EF	
AgNPs@g-C$_3$N$_4$	2.36%	MB	10^{-12}	1.4×10^8	1
Fe$_3$O$_4$/GO/Ag	6.90%	MB	10^{-9}	/	2
AgNPs/GO/g-CN	10.70%	MB	10^{-12}	6.59×10^8	3
CNF- Cu$_2$O/Ag	13.07%	MB	10^{-8}	4.0×10^4	4
Ag/GO	30.84	MB	10^{-10}	/	5
ZnO/Ag	39.14%	MB	10^{-9}	6.2×10^6	6
Ag@Hct	50.89%	MB	10^{-12}	2.6×10^4	7
MNPs-MoS2@Au	68.84%	MB	10^{-9}	/	8
Au/Bi$_2$O$_3$	5.20%	MB	10^{-11}	9.2×10^6	this work

1 Ag nanoparticles/g-C$_3$N$_4$.[12]

2 Fe$_3$O$_4$/GO/Ag composite microspheres.[13]

3 Ag nanoparticles /GO/g-CN nanohybrids.[14]

4 Cu$_2$O/Ag heterostructures within the cellulose nanofibrils (CNFs) network.[15]

5 Ag nanocubes/GO composites.[16]

6 ZnO nanoplates/Ag nanoparticles.[17]

7 spherical Ag/synthetic hectorite(Hct) nanomaterials.[18]

8 gold nanoparticles (AuNPs) grown on a magnetic sphere (MNPs)-MoS$_2$ microflower composite.[19]

Table S5. Peak fitting table of O 1s in Bi$_2$O$_3$.

Name	Peak BE	Height CPS	Height Ratio	Area CPS.eV	Area Ratio	FWHM fit param (eV)	L/G Mix(%) Product	Tail Mix (%)	Tail Height (%)	Tail Exponent
O1s Scan A	529.52	20164.61	0.95	53366.17	0.73	1.9	91.6	100	0	19.3813
						0.5 : 3.5				
O1s Scan B	531.01	21716.06	1	48777.45	1	1.44	1.11	100	0	19.6366
						0.5 : 3.5				

Table S6. Peak fitting table of O 1s in 5.20%Au/Bi$_2$O$_3$.

Name	Peak BE	Height CPS	Height Ratio	Area CPS.eV	Area Ratio	FWHM fit param (eV)	L/G Mix(%) Product	Tail Mix (%)	Tail Height (%)	Tail Exponent
O1s Scan A	529.55	40164.61	1	95085.96	1	1.9	0	0	100	0.0551
						0.5 : 3.5				
O1s Scan B	530.76	13716.06	0.34	41931.1	0.44	1.87	75.26	2.59	97.50	0.0389
						0.5 : 3.5				

Reference

[1]   E.C. Le Ru, E. Blackie, M. Meyer, P.G. Etchegoin, Surface Enhanced Raman Scattering Enhancement Factors: A Comprehensive Study, J. Phys. Chem. C 111 (2007) 13794–13803. https://doi.org/10.1021/jp0687908.

[2]   G.-N. Xiao, S.-Q. Man, Surface-enhanced Raman scattering of methylene blue adsorbed on cap-shaped silver nanoparticles, Chem. Phys. Lett. 447 (2007) 305–309. https://doi.org/10.1016/j.cplett.2007.09.045.

[3]   C. Li, Y. Huang, K. Lai, B.A. Rasco, Y. Fan, Analysis of trace methylene blue in fish muscles using ultra-sensitive surface-enhanced Raman spectroscopy, Food Control 65 (2016) 99–105. https://doi.org/10.1016/j.foodcont.2016.01.017.

[4]   O. Prakash, S. Kumar, P. Singh, V. Deckert, S. Chatterjee, A.K. Ghosh, R.K. Singh, Surface-enhanced Raman scattering characteristics of CuO : Mn/Ag heterojunction probed by methyl orange: effect of Mn^{2+} doping, J. Raman Spectrosc. 47 (2016) 813–818. https://doi.org/10.1002/jrs.4904.

[5]   J. Chen, K. Sun, Y. Zhang, D. Wu, Z. Jin, F. Xie, X. Zhao, X. Wang, Plasmonic MoO_2 nanospheres assembled on graphene oxide for highly sensitive SERS detection of organic pollutants, Anal. Bioanal. Chem. 411 (2019) 2781–2791. https://doi.org/10.1007/s00216-019-01751-z.

[6]   X. Zhou, X. Zhao, S. Gu, F. Xie, X. Wang, Z. Tang, Sulfur doped MoO_2 hollow nanospheres as a highly sensitive SERS substrate for multiple detections of organic pollutants, Anal. Methods 13 (2021) 2679–2687. https://doi.org/10.1039/D1AY00502B.

[7]   X. Wang, J. Li, X. Gao, Y. Shen, A. Xie, Ordered CdSe-sensitized TiO_2 inverse opal film as multifunctional surface-enhanced Raman scattering substrate, Appl. Surf. Sci. 463 (2019) 357–362. https://doi.org/10.1016/j.apsusc.2018.08.216.

[8]   B. Liu, K. Wang, B. Gao, J. Lu, H. Li, X. Zhao, TiO_2-Coated Silica Photonic Crystal Capillaries for Plasmon-Free SERS Analysis, ACS Appl. Nano Mater. 2 (2019) 3177–3186. https://doi.org/10.1021/acsanm.9b00492.

[9]   M. Liu, W. Liu, W. Zhang, P. Duan, M. Shafi, C. Zhang, X. Hu, G. Wang, W. Zhang, π-Conjugated Small Organic Molecule-Modified 2D MoS_2 with a Charge-Localization Effect Enabling Direct and Sensitive SERS Detection, ACS Appl. Mater. Interfaces 14 (2022) 56975–56985. https://doi.org/10.1021/acsami.2c17277.

[10]   P. Ren, W. Zhou, X. Ren, X. Zhang, B. Sun, Y. Chen, Q. Zheng, J. Li, W. Zhang, Improved surface-enhanced Raman scattering (SERS) sensitivity to molybdenum oxide nanosheets via the lightning rod effect with application in detecting methylene blue, Nanotechnology 31 (2020) 224002. https://doi.org/10.1088/1361-6528/ab758b.

[11]   Y. Peng, C. Lin, Y. Li, Y. Gao, J. Wang, J. He, Z. Huang, J. Liu, X. Luo, Y. Yang, Identifying infectiousness of SARS-CoV-2 by ultra-sensitive SnS_2 SERS biosensors with capillary effect, Matter 5 (2022) 694–709. https://doi.org/10.1016/j.matt.2021.11.028.

[12]   S. Li, P. Liang, Q. Chen, B. Sun, Z. Shang, J. Huang, M. Zou, X. Qi, J. Wu, One-pot fabrication of $Mo_{1-x}W_xS_2$ alloy nanosheets as SERS substrates with highly Raman enhancement effect and long-term stability, Spectrochim. Acta. A. Mol. Biomol. Spectrosc. 279 (2022) 121465. https://doi.org/10.1016/j.saa.2022.121465.

[13]   J. He, G. Song, X. Wang, L. Zhou, J. Li, Multifunctional magnetic Fe_3O_4/GO/Ag composite microspheres for SERS detection and catalytic degradation of methylene blue and ciprofloxacin, J. Alloys Compd. 893 (2022) 162226. https://doi.org/10.1016/j.jallcom.2021.162226.

[14]   S. Santhoshkumar, E. Murugan, Rationally designed SERS AgNPs/GO/g-CN nanohybrids to detect methylene blue and Hg^{2+} ions in aqueous solution, Appl. Surf. Sci. 553 (2021) 149544. https://doi.org/10.1016/j.apsusc.2021.149544.

[15]   Y. Luo, L. Xing, C. Hu, W. Zhang, X. Lin, J. Gu, Facile synthesis of nanocellulose-based Cu_2O/Ag heterostructure as a surface-enhanced Raman scattering substrate for trace dye detection, Int. J. Biol. Macromol. 205 (2022) 366–375. https://doi.org/10.1016/j.ijbiomac.2022.02.102.

[16]   J. He, X. Li, J. Li, Facile construction of silver nanocubes/graphene oxide composites for highly sensitive SERS detection of multiple organic contaminants by a portable Raman spectrometer, J. Environ. Chem. Eng. 10 (2022) 108278. https://doi.org/10.1016/j.jece.2022.108278.

[17]   T.T.H. Pham, X.H. Vu, N.D. Dien, T.T. Trang, T.T.K. Chi, P.H. Phuong, N.T. Nghia, Ag nanoparticles on ZnO nanoplates as a hybrid SERS-active substrate for trace detection of methylene blue, RSC Adv. 12 (2022) 7850–7863. https://doi.org/10.1039/D2RA00620K.

[18]   C.P. Fu, K.J. Li, J.Y. He, W.H. Yu, C.H. Zhou, Controlled fabrication of Ag@clay nanomaterials for ultrasensitive and rapid surface-enhanced Raman spectroscopic detection, Anal. Methods 15 (2023) 1001–1015. https://doi.org/10.1039/D2AY01262F.

[19]   H. Lai, G. Ma, W. Shang, D. Chen, Y. Yun, X. Peng, F. Xu, Multifunctional magnetic sphere-MoS$_2$@Au hybrid for surface-enhanced Raman scattering detection and visible light photo-Fenton degradation of aromatic dyes, Chemosphere 223 (2019) 465–473. https://doi.org/10.1016/j.chemosphere.2019.02.073.